

ORB-SLAM3-Enhanced Autonomous Toy Drones: Pioneering Indoor Exploration

Murad Tukan¹ and Fares Fares² and Yotam Grufinkle³ and Ido Talmor⁴ and
and Loay Mualem⁵ and Vladimir Braverman⁶ and Dan Feldman⁷

Abstract—Navigating toy drones through uncharted GPS-denied indoor spaces poses significant difficulties due to their reliance on GPS for location determination. In such circumstances, the necessity for achieving proper navigation is a primary concern. In response to this formidable challenge, we introduce a real-time autonomous indoor exploration system tailored for drones equipped with a monocular RGB camera.

Our system utilizes *ORB-SLAM3*, a state-of-the-art vision feature-based SLAM, to handle both the localization of toy drones and the mapping of unmapped indoor terrains. Aside from the practicability of *ORB-SLAM3*, the generated maps are represented as sparse point clouds, making them prone to the presence of outlier data. To address this challenge, we propose an outlier removal algorithm with provable guarantees. Furthermore, our system incorporates a novel exit detection algorithm, ensuring continuous exploration by the toy drone throughout the unfamiliar indoor environment. We also transform the sparse point to ensure proper path planning using existing path planners.

To validate the efficacy and efficiency of our proposed system, we conducted offline and real-time experiments on the autonomous exploration of indoor spaces. The results from these endeavors demonstrate the effectiveness of our methods.

I. BACKGROUND

Unmanned aerial vehicles (UAVs) have gained popularity over recent years for their wide array of applications, including aerial photography [LY12], surveillance [SJPP09], environmental monitoring [AdOdSF22], disaster response [HK19], and search and rescue missions [EEW13].

An essential goal within the realm of UAVs (Unmanned Aerial Vehicles) is to operate in close proximity to objects and navigate through environments that pose challenges for both humans and traditional aircraft. In these scenarios, compact UAVs, such as Toy-Sized [JFA⁺22] ones, play a

significant role. Such agents usually weigh less than 250 grams, due to regularization and safety issues, equipped with a monocular camera, for example, a Tello drone. Nevertheless, achieving autonomous exploration in GPS-denied unknown environments remains a formidable challenge for such agents. To accommodate proper exploration, one needs to account for (i) mapping the environment and (ii) using a proper path planner to move the agent from its current position to some goal point.

A. Mapping the Environment

Employing an autonomous exploration system for toy drones requires mapping the environment for proper localization and navigation through the environment. Next, we discuss widely used robotic mapping systems.

LiDAR-based systems. *LiDAR* sensors are technically laser beams measuring distances that can be utilized to produce a 3D map (or equivalently 2D map) of the surroundings [GZW⁺18], [CLHZ19], [IRS⁺22]. These systems not only generate precise maps of the surroundings but also perform simultaneous robot localization within the map. One significant drawback of such systems is that the cost of involved *LiDAR* sensors can be relatively high, potentially restricting their use in certain applications.

Vision-SLAM-based systems. Unlike *LiDAR*-generated maps, *SLAM*-generated maps can be represented in various forms, such as 2D or 3D grids, point clouds, or feature-based representations. Such maps are being created and updated in an incremental fashion as the agent moves through them. These *SLAM*-systems have shown promising results in the field of indoor exploration. For example, *RGB-D SLAM* [HKH⁺10] was utilized in an autonomous exploration system of unknown indoor environments via a novel exploration strategy exploiting the number of features and their distribution uniformity score in 3D [EZL⁺22]. While *RGB-D SLAM*-based systems allow for more detailed and accurate mapping due to the additional depth of information, their need comes with the existence of lighting conditions or where depth information is critical (e.g., robotics for object avoidance) via the use of depth cameras. When the usage of lightweight and efficient *SLAM* systems for real-time applications is a requirement, such systems are not ideal.

As for monocular RGB-camera *SLAM*-based systems, *LSD-SLAM* [ESC14] is a natural candidate for its scalable mapping, i.e., its ability to handle environments with varying scales. This system was utilized in [vSUE⁺17] to estimate the trajectory of the agent as well as ensure a semi-dense

¹ Murad Tukan is with DataHeroes, Israel murad@dataheroes.ai

² Fares Fares is with the Robotics and Big Data lab, University of Haifa, Haifa, Israel faresfares.cs@gmail.com

³ Yotam Grufinkle is with the Robotics and Big Data lab, University of Haifa, Haifa, Israel yotam706@gmail.com

⁴ Ido Talmor is with the Robotics and Big Data lab, University of Haifa, Haifa, Israel ifw.talmor@gmail.com

⁵ Loay Mualem is with the Computer Science Department, University of Haifa, Haifa, Israel, and with DataHeroes, Israel loaymua@gmail.com

⁶ Vladimir Braverman is with the Computer Science Department, Rice University, Houston Texas, USA vb21@rice.edu

⁷ Dan Feldman is with the Robotics and Big Data lab, University of Haifa, Haifa, Israel dannyf.post@gmail.com

* This work has been submitted to the IEEE for possible publication. Copyright may be transferred without notice, after which this version may no longer be accessible.

representation of the environment of the agent. While such a *SLAM* system can operate with minimal hardware such as a simple cheap monocular camera, the computational requirements of such a system may vary depending on the scale of the environment.

ORB-SLAM3 [CER⁺21]. This *SLAM* variant exhibits distinct advantages when compared to *LSD-SLAM* and *RGB-D SLAM*, particularly in terms of its robustness. It excels even in challenging scenarios marked by fluctuating lighting conditions and the presence of dynamic objects, among other complexities. Furthermore, *ORB-SLAM3* stands out as a cost-effective solution since it does not necessitate the use of additional high-cost sensors like *LiDAR*. Lastly, it is well-suited for applications where minimizing latency is paramount, providing a significant edge over other systems, such as *LSD-SLAM*, known for its computational intensity.

B. Path Planning

Path planning represents a pivotal challenge in the field of robotics. Its primary objective is to discover a viable route from an initial state to a desired final state while ensuring that the path avoids any potential obstacles. The principal difficulty arises from the typically vast and intricate search space that needs to be explored, especially when dealing with continuous problems. A common strategy employed to address this challenge is the strategic sampling of state configurations, with the attempt to uncover a feasible path. In practice, sampling-based path planning methods, such as Rapidly-exploring Random Trees (RRTs) [LaV98] and Probabilistic Roadmaps (PRMs), have gained widespread popularity as effective choices for navigating this intricate terrain leading to a vast array of variants of such path planners [LaV98], [KF10], [INM⁺12], [WvdB13], [SH16], [PD21], [TMFP22]. Traditionally in the field of path planning, the state space is composed mainly of two sets – the free space and the space of obstacle states where the latter is composed of fully bounded bodies (e.g., polytopes, convex bodies, etc.). In the context of *ORB-SLAM3*, obstacles are not represented by fully bounded bodies, but rather a sparse set of points. Thus, this prompts the question of whether **is it possible to maneuver the obstacle through such representation while ensuring collision avoidance?**

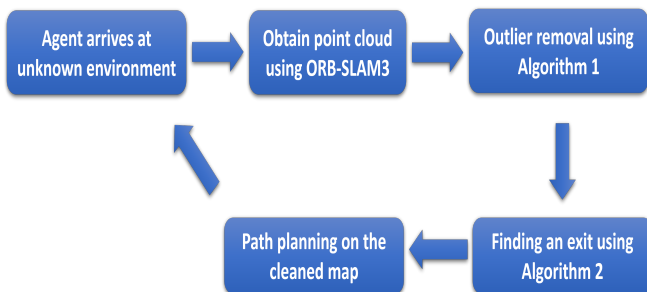


Fig. 1: An overview of our system’s pipeline.

II. OUR CONTRIBUTION

In this work, we provide a real-time autonomous exploration system in an indoor GPS-denied environment using a toy drone equipped with a single RGB monocular camera based on *ORB-SLAM3*. Problems arising towards such a goal consist of the lack of accurate positioning of the agent, the occurrence of noisy features grasped by *ORB-SLAM3* [CLX20], and adjusting path planners to sparse point clouds. In this context, there is no clear distinction between an obstacle point and a noisy point. This raises the question:

Is it possible to provide a real-time *ORB-SLAM3* based exploration system in indoor GPS-denied environments while adapting path planners to operate with sparse representation of such maps?

To that end, we answer the above question in the affirmative, where our contribution is four-fold:

- (i) Detecting and removing outliers (noise) via optimizing a submodular function with theoretical guarantees.
- (ii) Developing a 2D representation of the point cloud generated by *ORB-SLAM3* for finding goal (exit) points leading to exploration of unknown environments.
- (iii) Transforming sparse point clouds to a composition of free and obstacle states, thus allowing path planners to handle sparse data.
- (iv) Open code of our proposed system [Cod23].

III. SYSTEM

A. Key Idea

Given a lightweight toy drone (< 100gr) equipped with only a monocular RGB camera, the purpose of this work is to provide an autonomous system for state-space exploration of a low-cost drone utilizing a feature-based tracking and positioning system, namely, *ORB-SLAM3*.

***ORB-SLAM3* related problems.** First notice that *ORB-SLAM3* generates a sparse point cloud representing the local environment of the agent, referred to as \mathcal{M} . Traditionally, \mathcal{M} is represented via a composition of two sets of states, one reserved for the free states (obstacle-free locations), and the other set is for obstacles that are usually defined by dense bodies. An example of such representation is an occupancy grid [Elf89], [CC07]. While such a representation eases the task of navigating an agent through \mathcal{M} , recall that in our context \mathcal{M} is represented by a sparse set of points. As a result, the agent is faced with the added challenge of maneuvering through \mathcal{M} for multiple reasons.

For example, sparse representations of the data make the task of distinguishing between different obstacles harder, since the barrier between pairs of close obstacles is either under-sampled or poorly represented. As a byproduct of this, a completely dense obstacle is depicted as having a sufficiently large gap or opening, resulting from the incomplete capture of essential features, allowing the agent to pass through.

Bear in mind that *ORB-SLAM3* is prone to noisy samples, making the goal of navigation even harder to achieve. Such

noisy samples can occur due to illumination, reflective surfaces, etc. This is in addition to the *ORB-SLAM3* incapability of grasping enough features to represent either a closed window or a white blank wall. In summary, our *ORB-SLAM3*-based navigation system, faces three major problems:

- Existence of outliers.
- Finding goal points to navigate to.
- Path planning through sparse point clouds (*ORB-SLAM3* generated features).

Assumptions. To ensure autonomous navigation with *ORB-SLAM3*, the only assumption we require is that any environment has enough features to be grasped by *ORB-SLAM3*, in order to adequately represent the environments that our agent (e.g., drone) is passing through.

Notations. The following notations will be used throughout the paper. For any set of points $X \subseteq \mathbb{R}^d$, let $|X|$ denote the cardinality of X . For any positive integer n , let $[n]$ denote the set $\{1, 2, 3, \dots, n\}$. Finally, we let (A, v) denote an affine subspace (a linear subspace that does not necessarily pass through the origin of \mathbb{R}^3) where $A \in \mathbb{R}^{3 \times 2}$ is an orthonormal matrix and $v \in \mathbb{R}^3$ is its translation from the origin.

The steps of our system are illustrated in Figure 1. In the following subsections, we dive into each of the components that compose our system.

B. Outlier Removal

To address the challenge of capturing noisy features, we resort to subset selection methodologies. Note that subset selection techniques have gained much success throughout various fields, e.g., classification [MSSW18], [TMF20], [TBFR21], [MTBR23], clustering [BLK18], [ZTT20], [JTMF20], [TWZ⁺22], [TBD23], function fitting [MTP⁺22].

Different from prior work utilizing subset selection techniques, in this paper, we utilize such methods for identifying and eliminating outliers, specifically via employing *minimax optimization* for a *jointly-submodular* function. Recently, submodular functions have gained increasing interest in many machine learning and robotics problems, e.g., [ZTPT22], [MF22], [MF23], [MEFK23], [SRZT21]. In this paper, we use *minimax jointly-submodular* function optimization to remove outliers in the point cloud generated by *ORB-SLAM3*.

a) Minimax Submodular Optimization: We start with the property of *jointly-submodular* functions. Given an element u and two ground sets \mathcal{N}_1 and \mathcal{N}_2 , we denote by $f(u | S) \triangleq f(S \cup \{u\}) - f(S)$ the marginal contribution of the element u to the set S . The function f is *jointly-submodular* if for every two sets $S \subseteq T \subseteq \mathcal{N}_1 \cup \mathcal{N}_2$ and element $u \in (\mathcal{N}_1 \cup \mathcal{N}_2) \setminus T$, it holds that

$$f(u | S) \geq f(u | T).$$

Formally speaking, given two disjoint sets $\mathcal{N}_1, \mathcal{N}_2$, where each set is a copy of the point cloud generated by *ORB-SLAM3*, and two sets $X \subseteq \mathcal{N}_1, Y \subseteq \mathcal{N}_2$, we define “outliers

score” as follows.

$$f(X \cup Y) = \sum_{v \in \mathcal{N} \setminus X} \max_{u \in Y} s_{u,v} - \frac{1}{|\mathcal{N}_2|} \sum_{u \in Y} \sum_{v \in Y} s_{u,v} + \lambda \cdot |X|, \quad (1)$$

where $s_{u,v}$ is a “distance score” defined by $s_{u,v} = 1 - 1/d(u,v)$ —here, $d(u,v)$ represents the Euclidean distance between points u, v . A similar distance score was used by Mualem et al. [MEFK23], who also showed that (1) is a non-negative *jointly-submodular* function.

The function (1) consists of three terms. The first term represents a variation of the well-known Facility Location¹ function, which captures the representativeness of the set Y . The second term ensures the diversity of the chosen points, and the last term controls the number of detected outliers. Roughly speaking, we aim to find a set of points $\mathcal{N}_1 \setminus X$ that is good with respect to every representative set Y of some given size k in the sense that every point in Y is close to at least one point of $\mathcal{N}_1 \setminus X$. Thus, we have to (approximately) solve the following optimization problem.

$$\min_{X \subseteq \mathcal{N}_1} \max_{\substack{Y \subseteq \mathcal{N}_2 \\ |Y| \leq k}} f(X \cup Y). \quad (2)$$

b) Method: Maximizing submodular functions is NP-hard [Fei98]. However, it is possible to approximately optimize Equation (2) using Algorithm 1 (due to [MEFK23]). See Theorem 1 for the (informal) theoretical guarantee of this algorithm.

Overview of Algorithm 1. First, we note that X_0 in our context is an empty set since $f(\emptyset) = 0$; see Line 1. The algorithm then finds a representative set of points of size at most k from the whole data by optimizing the maximization component (akin to finding a geographical k -center from the data), aiming to expand its exploration of inliers; see Line 3. Specifically speaking, for every $i \in [|\mathcal{N}_1| + 1]$ at Lines 3–4, a submodular optimization oracle is utilized to find a subset Y_i containing at most k items of \mathcal{N}_2 that represent the remaining items of $\mathcal{N}_1 \setminus X_{i-1}$. We then find a subset X'_i of items from \mathcal{N}_1 that are close to Y_i , and add them to X_{i-1} to get the new set X_i ; see Lines 5–10.

The algorithm repeats this procedure until $X'_i \subseteq X_{i-1}$ (guaranteed to occur at some iteration). In our experiments, we employ the conventional Greedy Algorithm [NWF78], [MF22] as our maximization oracle \mathcal{O} , which ensures a guaranteed approximation of $\alpha = 1 - 1/e$. To visualize our Outlier Removal approach, we refer the reader to Figure 3c.

Theorem 1 (Informal version of Theorem 3.3 [MEFK23]): For an appropriate choice of the parameter β , Algorithm 1 returns a set $\hat{X} \subseteq \mathcal{N}_1$ such that $\max_{Y \in \mathcal{F}_2} f(\hat{X} \cup Y)$ is lower bounded by τ and upper bounded by $O(\alpha \sqrt{|\mathcal{N}_1|}) \cdot \tau$, where $\tau \triangleq \min_{X \subseteq \mathcal{N}_1} \max_{Y \in \mathcal{F}_2} f(X \cup Y)$.

C. Exit Detection

Following the outlier removal procedure concerning the local environment \mathcal{M} of the agent (as described in the

¹A Facility Location function represents the cost of a particular placement of facilities as a function of transportation costs and other factors.

Algorithm 1: Iterative X Growing

Input: A pair of sets of points $\mathcal{N}_1, \mathcal{N}_2 \subseteq \mathbb{R}^3$, a submodular maximization oracle \mathcal{O} , and number of centers k .

Output: A subset $S \subseteq \mathcal{N}_1$ of inliers.

- 1: Use an algorithm for submodular minimization to find a set $X_0 \in \arg \min_{X \subseteq \mathcal{N}_1} f(X)$
 - 2: **for** $i = 1$ **to** $|\mathcal{N}_1| + 1$ **do**
 - 3: Let $\mathcal{F}_2 := \{Y \mid Y \subseteq \mathcal{N}_2, |Y| \leq k\}$
 - 4: Use the oracle \mathcal{O} to find $Y_i \in \mathcal{F}_2$ maximizing $f(X_{i-1} \cup Y_i)$ up to a factor of α among all sets in \mathcal{F}_2
 - 5: Use an algorithm for submodular minimization to find a set $X'_i \in \arg \min_{X \subseteq \mathcal{N}_1} \beta f(X \cup X_{i-1}) + f(X \cup Y_i)$
 - 6: **if** $X'_i \subseteq X_{i-1}$ **then**
 - 7: **Return** X_{i-1}
 - 8: **else**
 - 9: Let $X_i \leftarrow X_{i-1} \cup X'_i$.
 - 10: **end if**
 - 11: **end for**
-

previous sub-section), we aim to find a point of interest that leads the agent to continue exploring the unknown environments.

To achieve this goal, it is important to acknowledge that the local environment data \mathcal{M} obtained through *ORB-SLAM3* can be unclear in distinguishing subsets of data points representing elements like walls, windows, or entrances due to inherent inaccuracies. For example, walls are often represented by non-linear point collections in 3D space, making it challenging to model them as linear subspaces accurately. This inaccuracy can result in significant deviations between the modeled subspaces and the actual wall structure. Furthermore, the presence of noisy data near entrances complicates the identification of exit points, whether they are open doors or elongated corridors.

a) LiDAR-based navigation system: Recall that in such systems, these challenges are typically mitigated thanks to the LiDAR method’s ability to measure the time it takes for reflected light to return to the receiver, which is a key feature of LiDAR sensors. With this functionality, it is possible to construct a precise 2D map that faithfully represents the local environment of the agent, as demonstrated in [HKRA16], while avoiding the presence of highly inaccurate samples. In contrast, *ORB-SLAM3* generates a sparse point cloud representation of the same environment, which may lack the same level of accuracy.

b) Reproducing “LiDAR” maps without any additional hardware: To alleviate this drawback, our goal is to generate a 2D representation of the provided map that preserves a structure similar to *LiDAR* maps, using solely a monocular

RGB-camera and *ORB-SLAM3*. To achieve this objective, two crucial components are required: (i) the agent’s position, and (ii) \mathcal{M} , which both are guaranteed by *ORB-SLAM3*. Next, we detail our algorithm that is designed to create maps with a structure closely resembling that of *LiDAR* maps. The ultimate goal is to identify a point of interest, referred to as an “exit point”, for the agent to navigate towards.

Overview of Algorithm 2. Given a set of n points $\mathcal{M} \subseteq \mathbb{R}^3$ representing a local map of our agent, the agent’s position $x \in \mathbb{R}^3$ and an affine subspace (A, v) which will be used to project the 3D map to 2D for easier processing, Algorithm 2 returns a point in 3D that lies on the affine subspace (A, v) representing an exit point. The algorithm starts by projecting the local map from 3D to 2D using the affine subspace (A, v) as well as the current agent’s position, namely, x ; see Line 1. Afterward, the angle between each point in the 2D projected map \mathcal{M}' and the 2D projected position x' of the agent is computed followed by creating 360 empty groups as depicted at Lines 2–3. The points in \mathcal{M}' are then dissected to 360 groups $(B_1, B_2, \dots, B_{360})$ such that a point $p \in \mathcal{M}'$ is assigned to a set B_i for some $i \in [360]$ if the angle between p and x' lies in the range $[i \cdot \pi/180, (i + 1) \cdot \pi/180]$; see Lines 5–13 and Figure 2. Moving forward, a 2D map is created such that the \mathcal{X} -axis represents angles between points in \mathbb{R}^2 and x' . Specifically speaking, we aim to create a map of 2D points, where a point is present at some (x, y) coordinates if $x \in [0, 2\pi]$ for some $i \in [360]$ such that $x \in B_i$ and $|B_i| > 1$. We then define y to be the average distance between points in B_i to x' . This is depicted at Lines 14–20 of Algorithm 2.

We are now able to find the angle that can lead to the exit by finding the largest continuous set of angles from the range $[0, 2\pi]$ such that there exists no point in L that has a x -axis coordinate in such segment. The angle of the exit point \bar{s} is set to be the median of the segment s ; see Line 22. The exit point in 2D is then set to be along the angle \bar{s} (Line 23) at a distance r (the mean norm of the projected points \mathcal{M}' as presented at Line 6). Finally, to map back to a 3D representation, we simply project back onto the affine space in its 3D form; see Lines 23–24.

D. Path Planning

After obtaining an exit point on some 2D plane in \mathbb{R}^3 , we proceed to find a collision-free path between the agent position and the proposed exit point.

Using the 2D map from Algorithm 2. Recall that *ORB-SLAM3*-generated maps differ from the data format typically processed by path planners. While the 2D map we created appears suitable for path planning due to its rigid lines, it simplifies by focusing on average distances within angle ranges. This neglects individual distances between the agent and points within each angle range, potentially leading to collisions by not accounting for obstacle positions along the agent’s path to the exit point.

From sparse to dense. Unlike traditional path planners that deal with dense obstacle representations, our approach addresses sparse point-based obstacle data from *ORB-*

Algorithm 2: EXIT-FINDER ($\mathcal{M}, x, (A, v)$)

Input: A set $\mathcal{M} \subseteq \mathbb{R}^3$ of n points representing the local map of our agent, the position $x \in \mathbb{R}^3$ of our agent, and an affine subspace (A, v)

Output: An exit point y that lies on the affine subspace (A, v)

```
#2D Projection
1: Let  $\mathcal{M}' := \{A^T(p - v) | p \in \mathcal{M}\}$  and let
    $x' := A^T(x - v)$ 
2: For every  $p \in \mathcal{M}'$ , Let  $\alpha(p) :=$  the radian angle
   between  $x'$  and  $p$ 
   #Dissect  $\mathcal{M}'$  into 360 bins
3: Let  $\mathcal{B} := \{B_i\}_{i=1}^{360}$  be a set of 360 empty bins
4: Let  $r := 0$ 
5: for every point  $p \in \mathcal{M}'$  do
6:    $r := r + \frac{1}{|\mathcal{M}'|} \|p\|_2$ 
7:   for every  $i \in [360]$  do
8:     if  $\alpha(p) \in [i \cdot \pi/180, (i + 1) \cdot \pi/180)$  then
9:        $B_i = B_i \cup \{p\}$ 
10:    break
11:   end if
12:   end for
13: end for
   #2D map production
14: Let  $L := \emptyset$ 
15: for every  $i \in [360]$  do
16:   if  $|B_i| > 1$  then
17:     Let  $\hat{d} := \frac{1}{|B_i|} \sum_{p \in B_i} \|p - x'\|_2$ 
18:      $L := L \cup \left\{ \left[ \frac{\beta}{180} \right] \middle| \beta \in [i \cdot \pi, (i + 1) \cdot \pi) \right\}$ 
19:   end if
20: end for
   #Finding an exit point
21: Let  $s :=$  the largest segment contained in  $[0, 2\pi]$ 
   such that no point in  $L$  has x-axis coordinate in the
   segment
22: Let  $\bar{s} :=$  the median element of  $s$ 
23:  $y' := x' + \begin{bmatrix} r \cos(\bar{s}) \\ r \sin(\bar{s}) \end{bmatrix}$ 
24:  $y := Ay' + v$ 
25: Return  $y$ 
```

SLAM3, where clear obstacle boundaries are lacking. Using a standard path planner on such maps can produce paths that pass through obstacles due to gaps in *ORB-SLAM3*'s obstacle representation. To resolve this, we propose a solution that combines K -means clustering and convex hull computation. After the outlier removal stage in our system, we cluster the map with a large number K of clusters (e.g., $K = 300$) using K -means, and then calculate a convex hull for each resulting cluster. This process creates our obstacle space, consisting of polytopes representing the obstacles.

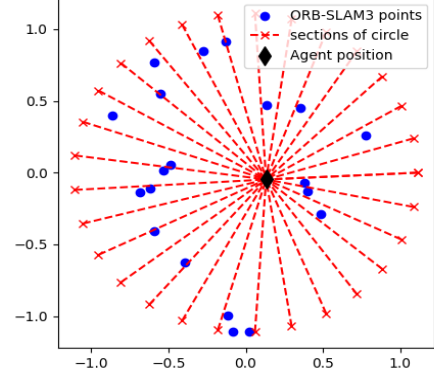


Fig. 2: Example of clustering *ORB-SLAM3* points to 30 groups based on their corresponding relative angle to the agent's position (highlighted by a black diamond). A point p is assigned to a circle sector $i \in [30]$ if its relative angle to the agent's position is in the range $[i * 2\pi/30, (i + 1) * 2\pi/30)$. Note that some of the groups might have no points at all hinging upon a possible entrance to an unexplored area.

With the set of obstacles above (set of convex hulls), we proceed to use the RRT path planner [LaV98] due to its simplicity and practicability.

Path refinement. The inherent randomness of RRT can lead to paths within the RRT tree that are occasionally unnecessarily complex, potentially resulting in longer routes when shorter ones are available. To tackle this problem, we devised a solution. For each sub-path of the path generated by RRT (between the agent's position and the exit point), starting at point A and ending at point B , we assess a single edge connecting A and B to determine its collision status. If the edge is collision-free, we replace the sub-path between A and B with this single edge.

IV. EXPERIMENTAL RESULTS

In this section, we describe our experiments, validating and assessing the quality of our proposed exploration system.

A. Experimental Settings

Hardware. Our experiments were conducted using a standard HP ZBook laptop with an Intel Core i7-10750H CPU @2.60GHzx12 and 32GB of RAM. Our agent is a DJI's Tello Drone ($< 90gr$, $< 100\%$), equipped with a small *RGB* monocular camera.

Software. Our system is implemented in C++ using *ORB-SLAM3* algorithm for localization and mapping.

Parameters and preprocessing. First, in the context of the outlier removal, i.e., Algorithm 1, we have found that $\beta := 1$, $k := 4$ and $\lambda := 0.6$ worked best throughout our experiments. Secondly, in the context of finding a point of exit, the 2D plane was set to be a plane that is parallel to

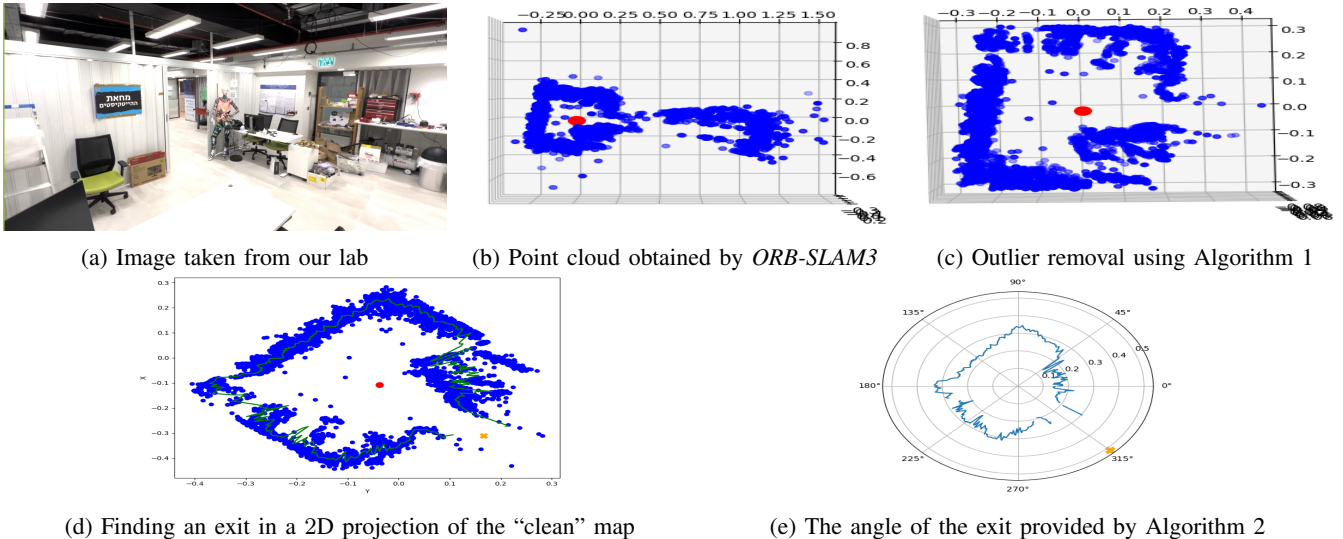


Fig. 3: Illustration of our system on a sub-environment of our lab (Figure 3a). Blue dots are *ORB-SLAM3* features, a red dot is the agent’s current position, green lines are the average distances at each angle from $[0, 359]$, and the yellow X is the generated exit point.

the ground – such a plane is generated by moving the drone in a triangular path obtaining three points while maintaining the same height from the ground. Finally, for the case of path planning, we have chosen $K := 1000$ (the number of centers) for our use of *K*-means clustering algorithm.

B. Offline Evaluation of Our Methods

In what follows, we assess the performance of our outlier removal and our exit finding algorithm.

Outlier Removal. Figure 3b illustrates the point cloud of a room generated by Tello Drone using *ORB-SLAM3*. Figure 3c demonstrates the outcome of our outlier removal process applied to Figure 3b – our method noticeably improves map quality by effectively reducing outliers.

Finding an Exit. After cleaning the *ORB-SLAM3* point cloud, Algorithm 2 is applied to find an exit point. In Figure 3d, a 2D projection of 3c is presented where the exit point is depicted by a yellow X. Recall that this is done by processing the map into an angular-based map as described in Algorithm 2; see Figure 3e.

C. Real-Time Experiment

Next, we describe and illustrate our real-time experiment. First, we placed a drone inside our lab (which consists of two rooms), with no prior knowledge of such an environment. The drone first lifts up, proceeding to scan the environment using *ORB-SLAM3* for feature extraction to represent the room as well as to localize the drone’s relative position. This is done, by rotating the drone 360 degrees compared to its initial pose, while going up and down during the rotation to maximize the number of obtained features. The drone then moves in a triangular path returning to its current position to generate a 2D plane which will be used by Algorithm 2.

We then employ Algorithm 1 to remove outliers followed by using Algorithm 2 to guide the drone in exploring

unknown areas. For effective path planning, we cluster the “clean” map using the *K*-means algorithm, and construct convex hulls for each of the clusters. Using this information, along with the exit point, as input for the RRT path planner, we obtain a path that navigates the drone from its current position to the next unknown environment. To ensure a smooth and simple path, the generated path undergoes refinement as described in subsection III-D.

Avoiding revisiting explored areas. We exploit the functionality of *ORB-SLAM3* to aid us in understanding whether a proposed exit point lies in an explored area. In such a case, prior to invoking Algorithm 2, the map undergoes further processing closing off certain areas that would prevent having an exit point in explored areas.

This whole procedure is iteratively applied until a previously defined criterion is satisfied, e.g., no exit points can be further explored. A result obtained during one of our real-time experiments (Figure 4), depicts a composition of the paths generated by our system that moves the Tello drone from one room inside the lab to outside our lab (see “Exit Point 2” at Figure 4). We refer the reader to our video of a similar experiment found in the supplementary material.

V. CONCLUSIONS AND FUTURE WORK

To the best of our knowledge, our low-cost ($< 100\$$) lightweight ($< 100\text{gr}$) vision featured-based monocular RGB autonomous drone navigation system is the first of its kind. We note that [KB23] proposed the use of *ORB-SLAM3* for navigating a Tello drone. However, no autonomous exploration system was provided.

Our system has shown efficacy throughout our experiments due to the provided outlier removal procedure, generation of points of interest (exit points), and proper transformation of “clean” map to ensure proper path planning using RRT.

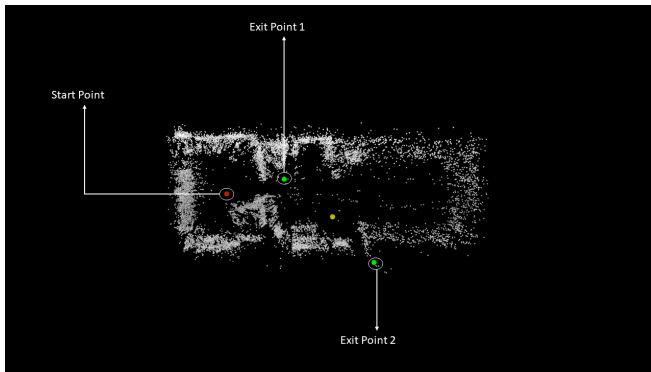


Fig. 4: A composition of paths guaranteed by our proposed system that moves the agent through a pair of rooms to an area outside the lab. The yellow point is a path point, red point is the drone’s initial position, and green points are exit points.

Future work includes adapting our system to operate only on Raspberry PI [JFA+22]. In addition, deep learning techniques have infiltrated this field, leading to promising results, e.g., [MGD+23]. This raises an additional future work of our proposed system to involve deep learning models combined with compression methods, e.g., [TMM22] that aim to ensure autonomous navigation under the constraint of very limited hardware such as Raspberry PI.

VI. ACKNOWLEDGMENTS

This work was partially supported by the Center for Cyber Law & Policy at the University of Haifa in conjunction with the Israel National Cyber Directorate in the Prime Minister’s Office.

REFERENCES

[AdOdSF22] Saeid Asadzadeh, Wilson Jose de Oliveira, and Carlos Roberto de Souza Filho. Uav-based remote sensing for the petroleum industry and environmental monitoring: State-of-the-art and perspectives. *Journal of Petroleum Science and Engineering*, 208:109633, 2022.

[BLK18] Olivier Bachem, Mario Lucic, and Andreas Krause. Scalable k-means clustering via lightweight coresets. In *Proceedings of the 24th ACM SIGKDD International Conference on Knowledge Discovery & Data Mining*, pages 1119–1127, 2018.

[CC07] Thomas Collins and JJ Collins. Occupancy grid mapping: An empirical evaluation. In *2007 mediterranean conference on control & automation*, pages 1–6. IEEE, 2007.

[CER+21] Carlos Campos, Richard Elvira, Juan J Gómez Rodríguez, José MM Montiel, and Juan D Tardós. Orb-slam3: An accurate open-source library for visual, visual-inertial, and multimap slam. *IEEE Transactions on Robotics*, 37(6):1874–1890, 2021.

[CLHZ19] Amauri B Camargo, Yisha Liu, Guojian He, and Yan Zhuang. Mobile robot autonomous exploration and navigation in large-scale indoor environments. In *2019 Tenth International Conference on Intelligent Control and Information Processing (ICICIP)*, pages 106–111. IEEE, 2019.

[CLX20] Like Cao, Jie Ling, and Xiaohui Xiao. Study on the influence of image noise on monocular feature-based visual slam based on ffdnet. *Sensors*, 20(17):4922, 2020.

[Cod23] Code. Open source code for all the algorithms presented in this paper, 2023. the authors commit to publishing upon acceptance of this paper or reviewer request.

[EEW13] David Erdos, Abraham Erdos, and Steve E Watkins. An experimental uav system for search and rescue challenge. *IEEE Aerospace and Electronic Systems Magazine*, 28(5):32–37, 2013.

[Elf89] Alberto Elfes. Using occupancy grids for mobile robot perception and navigation. *Computer*, 22(6):46–57, 1989.

[ESC14] Jakob Engel, Thomas Schöps, and Daniel Cremers. Lsd-slam: Large-scale direct monocular slam. In *European conference on computer vision*, pages 834–849. Springer, 2014.

[EZL+22] Amr Eldemiry, Yajing Zou, Yaxin Li, Chih-Yung Wen, and Wu Chen. Autonomous exploration of unknown indoor environments for high-quality mapping using feature-based rgb-d slam. *Sensors*, 22(14):5117, 2022.

[Fei98] Uriel Feige. A threshold of $\ln n$ for approximating set cover. *Journal of the ACM (JACM)*, 45(4):634–652, 1998.

[GZW+18] Haiming Gao, Xuebo Zhang, Jian Wen, Jing Yuan, and Yongchun Fang. Autonomous indoor exploration via polygon map construction and graph-based slam using directional endpoint features. *IEEE Transactions on Automation Science and Engineering*, 16(4):1531–1542, 2018.

[HK19] Hanno Hildmann and Ernő Kovacs. Using unmanned aerial vehicles (uavs) as mobile sensing platforms (msps) for disaster response, civil security and public safety. *Drones*, 3(3):59, 2019.

[HKH+10] P Henry, M Krainin, E Herbst, X Ren, and D Fox. Rgb-d mapping: Using depth cameras for dense 3d modeling of indoor environments. the 12th int. In *Symposium on Experimental Robotics (ISER)*, 2010.

[HKRA16] Wolfgang Hess, Damon Kohler, Holger Rapp, and Daniel Andor. Real-time loop closure in 2d lidar slam. In *2016 IEEE international conference on robotics and automation (ICRA)*, pages 1271–1278. IEEE, 2016.

[INM+12] Fahad Islam, Jauwairia Nasir, Usman Malik, Yasar Ayaz, and Osman Hasan. Rrt*-smart: Rapid convergence implementation of rrt* towards optimal solution. In *2012 IEEE international conference on mechatronics and automation*, pages 1651–1656. IEEE, 2012.

[IRS+22] Hasan Ismail, Rohit Roy, Long-Jye Sheu, Wei-Hua Chieng, and Li-Chuan Tang. Exploration-based slam (e-slam) for the indoor mobile robot using lidar. *Sensors*, 22(4):1689, 2022.

[JFA+22] Ibrahim Jubran, Fares Fares, Yuval Alfassi, Firas Ayoub, and Dan Feldman. Newton-pnp: Real-time visual navigation for autonomous toy-drones. In *2022 IEEE/RSJ International Conference on Intelligent Robots and Systems (IROS)*, pages 13363–13370. IEEE, 2022.

[JTMF20] Ibrahim Jubran, Murad Tukan, Alaa Maalouf, and Dan Feldman. Sets clustering. In *International Conference on Machine Learning*, pages 4994–5005. PMLR, 2020.

[KB23] Saira Khan and Abdul Basit. Vision-based monocular slam in micro aerial vehicle. *LC International Journal of STEM (ISSN: 2708-7123)*, 4(1):41–51, 2023.

[KF10] Sertac Karaman and Emilio Frazzoli. Incremental sampling-based algorithms for optimal motion planning. *Robotics Science and Systems VI*, 104(2):267–274, 2010.

[LaV98] Steven LaValle. Rapidly-exploring random trees: A new tool for path planning. *Research Report 9811*, 1998.

[LY12] Xin Li and Lian Yang. Design and implementation of uav intelligent aerial photography system. In *2012 4th International Conference on Intelligent Human-Machine Systems and Cybernetics*, volume 2, pages 200–203. IEEE, 2012.

[MEFK23] Loay Mualem, Ethan R Elenberg, Moran Feldman, and Amin Karbasi. Submodular minimax optimization: Finding effective sets. *arXiv preprint arXiv:2305.16903*, 2023.

[MF22] Loay Mualem and Moran Feldman. Using partial monotonicity in submodular maximization. *Advances in Neural Information Processing Systems*, 35:2723–2736, 2022.

[MF23] Loay Mualem and Moran Feldman. Resolving the approximability of offline and online non-monotone dr-submodular maximization over general convex sets. In *International Conference on Artificial Intelligence and Statistics*, pages 2542–2564. PMLR, 2023.

- [MGD⁺23] Alaa Maalouf, Yotam Gurfinkel, Barak Diker, Oren Gal, Daniela Rus, and Dan Feldman. Deep learning on home drone: Searching for the optimal architecture. In *2023 IEEE International Conference on Robotics and Automation (ICRA)*, pages 8208–8215. IEEE, 2023.
- [MSSW18] Alexander Munteanu, Chris Schwiigelshohn, Christian Sohler, and David Woodruff. On coresets for logistic regression. *Advances in Neural Information Processing Systems*, 31, 2018.
- [MTBR23] Alaa Maalouf, Murad Tukan, Vladimir Braverman, and Daniela Rus. Autocoreset: An automatic practical coreset construction framework. *arXiv preprint arXiv:2305.11980*, 2023.
- [MTP⁺22] Alaa Maalouf, Murad Tukan, Eric Price, Daniel M Kane, and Dan Feldman. Coresets for data discretization and sine wave fitting. In *International Conference on Artificial Intelligence and Statistics*, pages 10622–10639. PMLR, 2022.
- [NWF78] George L Nemhauser, Laurence A Wolsey, and Marshall L Fisher. An analysis of approximations for maximizing submodular set functions—i. *Mathematical programming*, 14:265–294, 1978.
- [PD21] Louis Petit and Alexis Lussier Desbiens. Rrt-rope: A deterministic shortening approach for fast near-optimal path planning in large-scale uncluttered 3d environments. In *2021 IEEE International Conference on Systems, Man, and Cybernetics (SMC)*, pages 1111–1118. IEEE, 2021.
- [SH16] Oren Salzman and Dan Halperin. Asymptotically near-optimal rrt for fast, high-quality motion planning. *IEEE Transactions on Robotics*, 32(3):473–483, 2016.
- [SJPP09] Eduard Semsch, Michal Jakob, Dušan Pavlicek, and Michal Pechoucek. Autonomous uav surveillance in complex urban environments. In *2009 IEEE/WIC/ACM International Joint Conference on Web Intelligence and Intelligent Agent Technology*, volume 2, pages 82–85. IEEE, 2009.
- [SRZT21] Guangyao Shi, Ishat E Rabban, Lifeng Zhou, and Pratap Tokekar. Communication-aware multi-robot coordination with submodular maximization. In *2021 IEEE International Conference on Robotics and Automation (ICRA)*, pages 8955–8961. IEEE, 2021.
- [TBD23] Murad Tukan, Eli Biton, and Roei Diamant. An efficient drifters deployment strategy to evaluate water current velocity fields. *arXiv preprint arXiv:2301.04216*, 2023.
- [TBFR21] Murad Tukan, Cenk Baykal, Dan Feldman, and Daniela Rus. On coresets for support vector machines. *Theoretical Computer Science*, 890:171–191, 2021.
- [TMF20] Murad Tukan, Alaa Maalouf, and Dan Feldman. Coresets for near-convex functions. *Advances in Neural Information Processing Systems*, 33:997–1009, 2020.
- [TMFP22] Murad Tukan, Alaa Maalouf, Dan Feldman, and Roi Poranne. Obstacle aware sampling for path planning. In *2022 IEEE/RSJ International Conference on Intelligent Robots and Systems (IROS)*, pages 13676–13683. IEEE, 2022.
- [TMM22] Murad Tukan, Loay Mualem, and Alaa Maalouf. Pruning neural networks via coresets and convex geometry: Towards no assumptions. *Advances in Neural Information Processing Systems*, 35:38003–38019, 2022.
- [TWZ⁺22] Murad Tukan, Xuan Wu, Samson Zhou, Vladimir Braverman, and Dan Feldman. New coresets for projective clustering and applications. In *International Conference on Artificial Intelligence and Statistics*, pages 5391–5415. PMLR, 2022.
- [vSUE⁺17] Lukas von Stumberg, Vladyslav Usenko, Jakob Engel, Jörg Stückler, and Daniel Cremers. From monocular slam to autonomous drone exploration. In *2017 European Conference on Mobile Robots (ECMR)*, pages 1–8. IEEE, 2017.
- [WvdB13] David J Webb and Jan van den Berg. Kinodynamic rrt*: Asymptotically optimal motion planning for robots with linear dynamics. In *Robotics and Automation (ICRA), 2013 IEEE International Conference on*, pages 5054–5061. IEEE, 2013.
- [ZTPT22] Lifeng Zhou, Vasileios Tzoumas, George J Pappas, and Pratap Tokekar. Distributed attack-robust submodular maximization for multirobot planning. *IEEE Transactions on Robotics*, 38(5):3097–3112, 2022.
- [ZTT20] Yu Zhang, Kanat Tangwongsan, and Srikanta Tirthapura.

Fast streaming k -means clustering with coresets caching.
IEEE Transactions on Knowledge and Data Engineering,
34(6):2740–2754, 2020.